DIRECTIONAL ENHANCEMENT OF COMPOSITE STRUCTURES ENERGY ABSORPTION USING MAGNETORHEOLOGICAL FLUIDS

Shen Hin Lim*,***, B. Gangadhara Prusty*, Garth Pearce*, Donald Kelly*, Rodney Thomson**,***
*School of Mechanical and Manufacturing Engineering, University of New South Wales, Sydney, Australia
**Advanced Composite Structures Australia Pty Ltd, Port Melbourne, Victoria, Australia
***Cooperative Research Centre for Advanced Composite Structures, Fishermans Bend, Victoria, Australia
shen.lim@unsw.edu.au;g.prusty@unsw.edu.au

Keywords: *magnetorheological fluids, composite, crashworthiness*

Abstract

The compatibility of magnetorheological (MR) fluids to directional enhancement of composite structures energy absorption has been investigated in this paper. This work is a part of CRC-ACS research program that aims to develop retrofit technologies for aged helicopters. Firstly, numerical parametric studies were conducted on identified design parameters of MR damper. This is followed by exploring the experimental data obtained from existing MR damper. The numerical studies showed that the piston head radius is the key dominant effect in providing high damping force. This, however, also resulted in large change of the MR damper weight due to significant increase of MR fluids volume, as compared to other design parameters. The analysis of experimental result shows that the damping force is equivalent to roughly two-fifths of the mean crushing force of an off-the-shelf composite tube with similar dimensions of the existing MR damper. MR fluids and damper show promising quality to improve composite structures as systems for crashworthiness.

1 Introduction

Aged helicopters are required to be remodelled and applied with retrofit technologies to meet the newer crashworthy standards during their service life, while not affecting other aspects of the helicopter. Hence, lightweight and crashworthy composite materials are strong candidate for these retrofit technologies [1], and this has led to extensive research on composite-based retrofit technologies. These composite-based retrofit technologies can be further enhanced with a hybrid material and/or other materials with rheological behaviour, such as magnetorheological (MR) and electrological fluids.

MR fluids are used for smart systems and have been increasingly popular in the last decade, as the rheological behaviour can be easily and accurately controlled by an external magnetic field [2]. The MR fluids anisotropic behaviour and its capability to achieve high yield stress has sparked its applications as a semi-active damper in civil engineering structures for earthquake mitigation [3–5] and also as the magnetorheological energy absorbers (MREAs) for crashworthy seats [6–7].

Dampers with MR fluids are chosen for earthquake related isolation of structures due to its low power requirements to dissipate vibratory energy in a structural system efficiently. A large number of research work and its application were focused on developing

an effective control of this highly nonlinear device and also modelling of multiple MR dampers [3–4]. Dyke et al. [3] proposed a clipped-optimal control strategy based on acceleration feedback and successfully reduced the peak displacements of a building as compared to an active linear control system. On the other hand, Yang et al. [4–5] proposed dynamic modelling for large-scale MR damper systems and showed the capability to achieve high damping force in a short time. The success from the intensive modelling exercise of MR dampers in civil engineering structures has initiated the potential of MR fluids in other applications in different areas such as aerospace and automobile industry, which include those restricted in size and weight.

MREAs acts as an alternative to the conventional energy absorbers, and allows the load-stroke profile to be adapted as a function of occupant weight or real-time crash load levels. Choi and Wereley [6] investigated the potential of MREAs under vibration and shock loads created from normal and crash landing situations and found them being superior to conventional passive hydraulic seats in both situations. Hiemenz et al. [7] achieved similar results and further conducted a study to measure the performance of the current MREAs based on vibration isolation and crashworthiness conditions. This study showed that the weight of the MREAs is a major issue for satisfactory performance in these conditions simultaneously, and hinted that further improvements are required to adopt MREAs as crashworthy seats. While current MREAs development showed limited applications, removing the MREAs limitations could escalate MR fluids application into other areas of crashworthiness systems.

The main focus of this paper lies on the investigation of the MR fluids compatibility to enhance the directional behaviour of structures energy absorption, and is an essential step towards the integration of MR fluids with the developed composite components to meet the crashworthiness requirements for the aged helicopters. This is a part of Cooperative Research Centre for Advanced Composite Structures (CRC-ACS) research program on Systems for Crashworthiness. Initially, parametric studies are conducted based on the identified MR damper design parameters, which are ratio of MR particle to the medium, dimensions of the piston head and the gap of flow channel between two electrodes. Similarly, the damping force, which is a key element in measuring the compatibility to enhancement of structures energy absorption, is also evaluated in the experiment using an existing MR damper from LORD Corporation [8].

The identification of design parameters, which is inclusive of the fundamental study of MR fluids and damper, is first offered in this paper. This is followed by comprehensive parametric studies of the identified design parameters in Section 3. The experimental setup and results are presented in Section 4 and Section 5. Finally, Section 6 covers the conclusion and future work.

2 Identification of MR Damper Design Parameters

MR fluids consist of micrometer-sized carbonyl iron particles dispersed at volume fractions usually of the order of 0.3 in silicone/other fluids. The diagrammatic illustration of the concept of MR fluids, and its anisotropic behaviour when the magnetic field is activated, is depicted in Fig. 1. The direction of the magnetic particle is perpendicular to the electromagnet. The behaviour of the magnetic particles is based on the volume fractions of the magnetic particles as well as inclusion of other additive particles, such as carbon nanotubes, fumed silica and organoclay. The inclusion of additive particles is aimed to increase dispersion stability [9].

MR fluids can also be accurately controlled by its viscosity, η_0 and is responsive within miliseconds of change in magnetic fields. MR fluids are non-Newtonian fluids and it is usually modelled by Bingham plastic model for high shear rate [9], which is governed by the equation below.

$$\tau = \tau_y(H) + \eta_0\dot{\gamma}, \tau > \tau_y \qquad (1)$$

where τ is shear stress, τ_y is yield stress based on H, which is magnetic field strength, and $\dot{\gamma}$ is the shear rate.
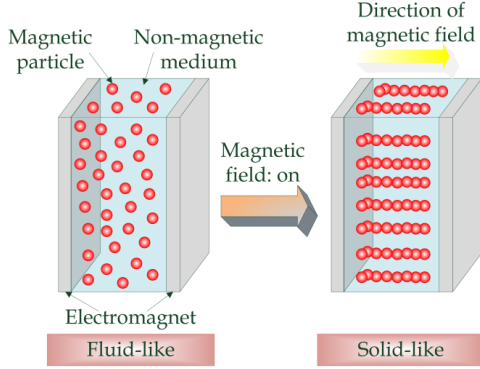
Fig. 1. Illustration of MR fluids concept in idle and active form

The mechanism of MR damper with the associated dimension parameters is illustrated in Fig.2. When the damper is activated, the active MR fluids is in between the gap of the flow channel d, shown between the electrodes located at the piston and the outside casing of the MR damper. The other dimensions of interest are piston head length, L and radius, R_1 while areas A_d and A_p represent the circumferential area of active MR fluid and piston head surface area respectively. The damping force created by MR fluids F_D, thus, becomes

$$F_D = C_{eq}v_0 + 2\pi R_1 L\tau_y (H) sign(v_0) \qquad (2)$$

where C_{eq} is off–state viscous damping coefficient and v_0 is the piston velocity.

The damping coefficient C_{eq} is in an uncontrollable form and is required to be derived using available design parameters. As MR damper is generally a pressure driven flow mode device, C_{eq} is derived from the evaluation of the velocity of fluid within the gap d. The damping coefficient C_{eq}, using the ratio $\bar{\delta}$, between the distance of laminar flow δ and gap d, is then offered by

$$C_{eq} = \frac{24\eta_0 LA_p^2}{A_d d^2 (1-\bar{\delta})^2 (2+\bar{\delta})} \qquad (3)$$

Design parameters are identified and are categorised into three different groups. First is the ratio of MR particle to the medium that is

represented by viscosity η_0 and yield stress of maximum applied current τ_y. The second group covers the dimensions of the piston head, which are the piston head length and radius L and R_1. The gap of the flow channel d is the final group of identified design parameters.
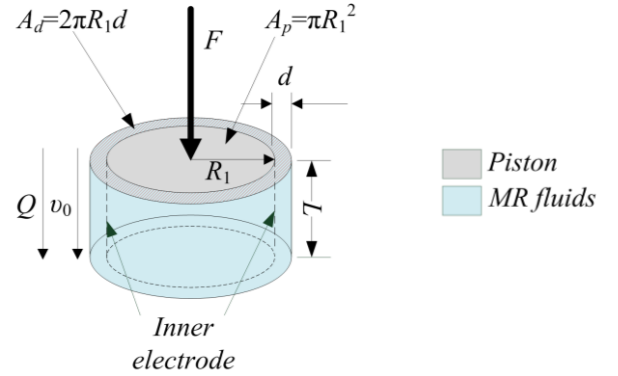
Fig. 2. Illustration of MR damper with design parameters of interest

3 Parametric Studies of Identified Design Parameters

In this section, the effect of the identified design parameters has been investigated. The magnetic field strength H, was varied from 0 to 100 Am^{-1} to provide variability to the yield stress and to examine the performance of the damping force. Similarly, the velocity v_0 was also varied from -200 to 200 mm/s. First, the viscosity η_0 and the yield stress τ_y that represent the ratio of MR particles to the medium were studied based on the resultant damping force. Three different types of MR fluids obtained from the LORD specification sheet [8], which were referred as C1, C2 and C3, were utilised and shown in Table 1.

Table 1. Three different configurations of MR fluids of MR fluids from LORD specification sheet [8]

	C1	C2	C3
Viscosity, η_0 (Pa·s)	0.042	0.092	0.28
Maximum yield stress, τ_{ymax} (MPa)	0.35	0.5	0.6
Piston head length, L (mm)		30	
Piston head radius, R_1 (mm)		20	
Gap of flow channel, d(mm)		1	

In this study, yield stress τ_y was also varied to the maximum yield stress $\tau_{y\max}$. Other design parameters, which were piston head length and radius, were constant for this parameter study in order to quantify the explored parameters effect.

The damping force distribution based on the parameters in Table 1 and velocity v_0 is shown in Fig. 3. The force F_D linearly increases with the increment of yield stress τ_y due to the linear relationship between force F_D and yield stress τ_y, as presented in Equation (2). Similarly, it also shows that force F_D distribution from C1 to C3 has indicates possible linearity effect with the increment of viscosity η_0 value. This is more distinctly shown in Fig. 4, when the yield stress τ_y was held constant at 0.22MPa. The viscosity η_0 also elevates the effect of H and thus MR fluids with the highest viscosity η_0 is the best option to achieve most effective damping force distribution with any velocity. The linear response due to the change in these parameters enables easier controllability of the MR damper design.

For the remaining parametric studies, the MR fluids with the lowest η_0 and τ_y were utilised to diminish their effect and to increase the studied parameters effect towards the resultant damping force. The effect of the piston head length and radius L and R_1 were examined and the values for all the parameters are presented in Tables 2 and 3. The length L was varied from 10 to 50 mm while the radius R_1 was varied from 5 to 40 mm for each of their corresponding parametric investigations.
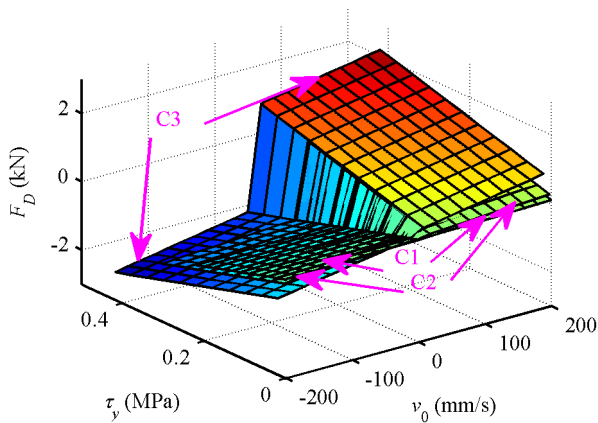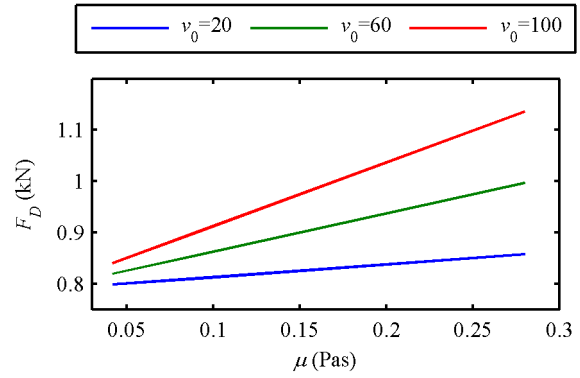
Fig. 4. The damping force distribution with constant τ_y based with υ_0 (in mm/s)

Table 2. The design parameters values for investigation of piston head length effect

	Min	Max
Viscosity, η_0 (Pa·s)	0.042	
Maximum yield stress, $\tau_{y\max}$ (MPa)	0.35	
Piston head length, L (mm)	10	50
Piston head radius, R_1 (mm)	20	
Gap of flow channel, d (mm)	1	

Table 3. The design parameters values for study of piston head radius effect

	Min	Max
Viscosity, η_0 (Pa·s)	0.042	
Maximum yield stress, $\tau_{y\max}$ (MPa)	0.35	
Piston head length, L (mm)	30	
Piston head radius, R_1 (mm)	5	40
Gap of flow channel, d (mm)	1	
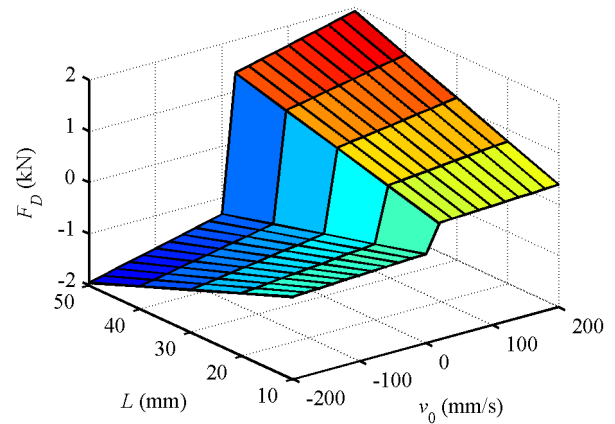
Fig. 5. The damping force distribution based on variations of L

Fig. 3. The damping force distribution based on variations of τ_y and v_0

The damping force distribution based on the yields stress and change in length L when the yield stress τ_y is set constant at 0.22MPa, is presented in Fig. 5. The length L has a dominant linear effect on the damping force F_D in Fig. 6. Using a set constant velocity v_0 at 20mm/s, the Fig. 6 illustrates that the linear effect by length L is not affected by different values of yield stress τ_y, and this also validates the independence of τ_y due to changes in L.
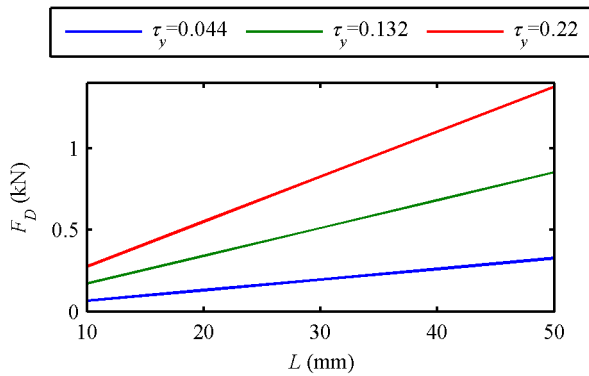
Fig. 6. The damping force distribution based on variations of L with constant τ_y (in MPa)

The damping force distribution with the change in radius R_1 when the yield stress τ_y is set constant at 0.22MPa is shown in Fig. 7. Conversely to length L, radius R_1 provides a non-linear effect to the damping force. This indicates that radius R_1 have more dominant effect on the force F_D.
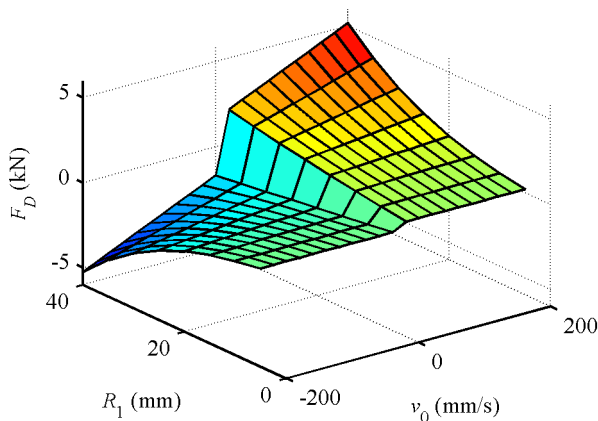
Fig. 7. The damping force distribution based on variations of R_1

To further quantify these effects while simplicity is maintained, yield stress τ_y and velocity v_0 were set constant at three different

settings, presented in Table 4. These settings were referred as D1, D2 and D3. The variations of length and radius L and R_1 were also given in Table 4. The resultant damping force distribution based on the change in L and R_1 for D1, D2 and D3 is shown in Fig. 8. In D1 case, both L and R_1 have similar dominant effect to the force F_D, despite the non-linear effect of R_1. The non-linear effect of R_1 becomes more dominant in D2 and D3, as compared to L. However, the piston head surface area A_p also undergoes the quadratic non-linear effect and consequently highly increases the weight of MR damper.

Table 4. The design parameters values for investigation of piston head length, L and radius, R_1 effects

		D1	D2	D3
Velocity , v_0 (mm/s)		10	10	50
Yield stress, τ_y (MPa)		0.22	0.42	0.42
Piston head	Min		10	
length, L (mm)	Max		50	
Piston head	Min		5	
radius, R_1 (mm)	Max		40	
Gap of flow channel, d			1	
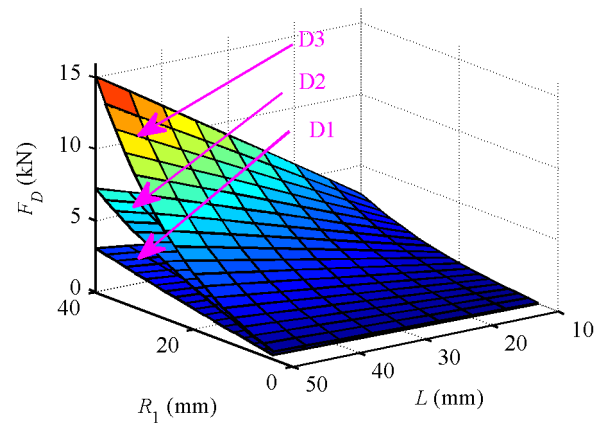
Fig. 8. The damping force distribution based on variations of L and R_1

The final design parameter, which is the gap of flow channel d, was examined with the corresponding values of parameters given in Table 5. In this parametric study, the distance of laminar flow δ was also examined. Fig. 9 shows the resultant damping force distribution based on the change in d, where Fig. 9(a) is based on F1 while Fig. 9(b) is based on F2. This indicates that distance δ has to be small as compared to d

to avoid turbulent force distribution. Further evaluation of this study shows that distance δ needs to be lower than $0.4d$ for consistent force distribution for a wide range of gap. The curvature at lower end of d is to ensure that the remaining distance, $d-\delta$, is enough for settling of the MR fluid flow at the edge of inner and outer electrodes.

Table 5. The design parameters values for study of gap of flow channel effect

		Min	Max
Viscosity, η_0 (Pa·s)		0.042	
Maximum yield stress, $\tau_{y\max}$ (MPa)		0.35	
Piston head length, L (mm)		30	
Piston head radius, R_1 (mm)		20	
Gap of flow channel, d (mm)		0.3	2
Distance of laminar	F1	0.4d	
flow, δ (mm)	F2	0.75d	

(a)

(b)
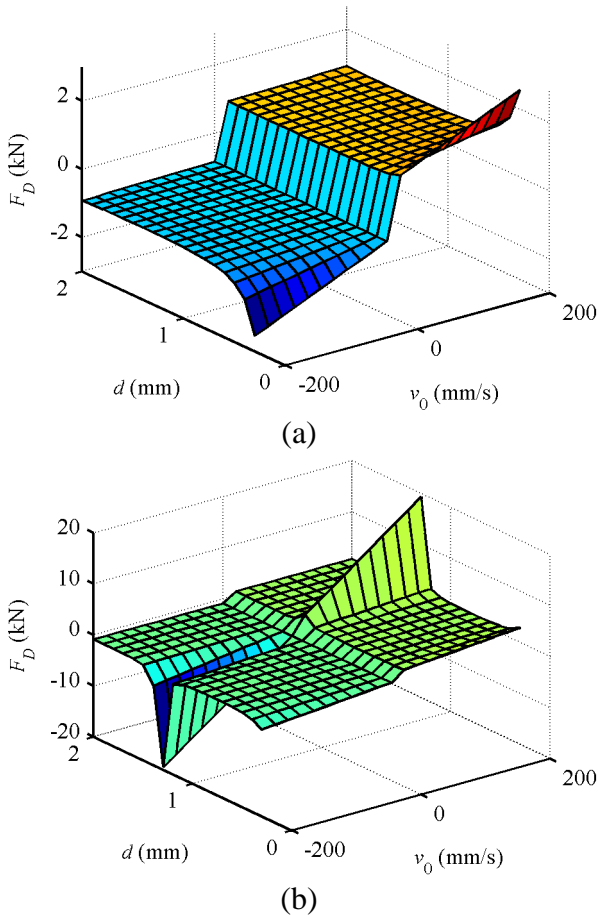
Fig. 9. The damping force distribution based on variations of d and (a) δ =0.4d and (b) δ =0.75d

4 Experimental Results

Experiments were conducted to investigate the response and damping force of an existing MR damper with variations of velocity v_0 and the induced current I, which controls the magnetic field H. The tests were conducted on a MR damper, RD-8041-1 and the induced current is controlled by a device called as Wonderbox, where both were purchased from the LORD Corporation [8]. The schematic of the experimental setup is shown in Fig. 10, where the inputs were the velocity v_0 and the induced current I. The MR damper is tested on two different universal testing machines (Instron), where one is a mechanically driven while the latter is a hydraulic driven machine, to cover a different range of velocities. The range set for the inputs was shown in Table 6. In this experimental study, the mechanically driven machine was referred as MD while the other was referred as HD machine.

The velocity increments of MD and HD machines are 1mm/s and 5mm/s respectively. Three different tests were conducted, which are tensile, compression and cyclic loading tests. The tensile and compression loading tests were carried out on the MD machine while the cyclic loading tests were carried out on the HD machine. The total maximum displacement travel for the actuator on the MD machine is 45mm. On the other hand, the cyclic loading is set to travel in a trapezoidal wave with the peak to peak distance of 40mm. For each test, the maximum damping force was used for the analysis of experimental results.
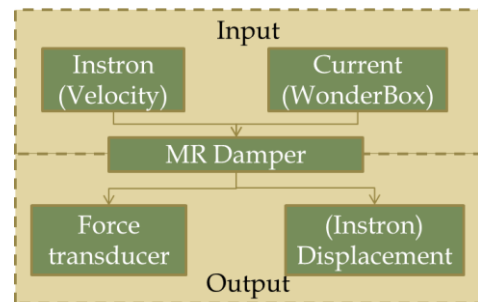
Fig. 10. The schematic of the experimental setup

Table 6. The input range for the experimental test of MR damper

	Min		Max	
	MD	HD	MD	HD
Velocity, v_0 (mm/s)	0	0	5	20
Current, I (A)	0		1.68	

The illustration of the force distribution of the MR damper tested on MD machine is shown in Fig. 11. Fig. 11(a) and Fig. 11(b) present the damping force distribution on the compression and tensile loading regimes. The magnitude of the force F_D was increased with the increment of velocity v_0 and current I in both tests successfully. The force distribution in both tests also coincides with the behaviour shown in the numerical parametric studies and the manufacturer's (LORD) specification sheet. However, both the loading tests had inconsistent force F_D with the increment of velocity occurring at the higher end set of current I. In agreement with the manufacturer's specifications, the effect of temperature on the type of loading is noticed. As depicted by the maximum force at v_0=5mm/s and I=1.68A, it is noticed that the higher magnitude of force F_D in the compression loading test, as compared to the tensile loading test.

The force F_D in the tensile loading test stabilised from velocity v_0=3mm/s for every set of current I. This was possibly due to the analysis at the lower end of the MR damper operating velocity range that is up to 200mm/s. The damping force distribution based on the cyclic loading tests is shown in Fig. 12. The data extracted from the manufacturer's (LORD) [8] specification sheet is depicted by the dotted lines at I=0A, I=0.5A and I=1A. The results from the cyclic loading test matched to those obtained from the manufacturer's specification. The distribution of force F_D is consistent in this experiment mainly due to the hydraulic operation of the HD machine together with the higher set of velocity range, as compared to tensile and compression loading tests.

(a)

(b)
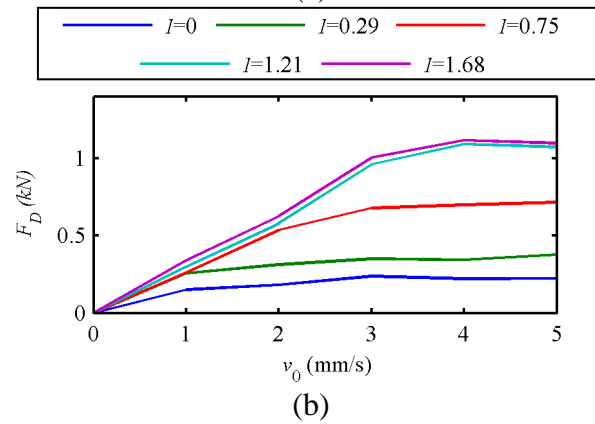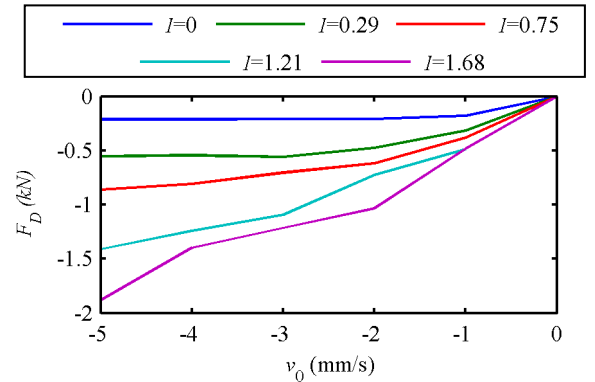
Fig. 11. The damping force distribution based on the (a) compression and (b) tensile loading tests (I is in A)
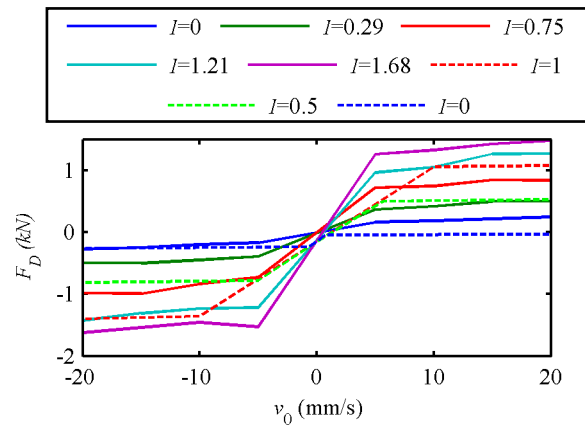
Fig. 12. The damping force distribution based on the cyclic loading test (I is in A and the dotted lines are extracted from manufacturer's specification sheet)

5 Possible Integration to Composite Structures

The damping force F_D from the tensile, compression and cyclic loading tests of the experiment study in the previous section was further evaluated in this section to measure the

compatibility of the MR damper to composite structures energy absorption quantitatively. First, the highest peak to peak forces from those loading tests, which were referred as tensile, compression and cyclic respectively, were extracted with their corresponding peak to peak distance travelled. These forces were produced by the highest input velocity and current input in each respective test. These forces were compared to the mean of the force, F_{tube} produced by crushing an off-the-shelf composite tube, and this mean force was named as $\bar{F}_{tube}$. The composite tube was a woven pre-preg ($0^o/90^o$ layup), 38.1mm inner diameter, 2mm thickness and 200mm height. Fig. 13 illustrates the comparison of peak to peak forces of compression, tensile and cyclic loading tests to the crushing force, F_{tube}. The force $\bar{F}_{tube}$ was 7.9kN. In comparison, the peak to peak forces from the compression and tensile loading tests are 23.72% and 13.79% of the force $\bar{F}_{tube}$ while cyclic loading is 38.06% of the force $\bar{F}_{tube}$. This shows that the MR damper is capable to improve the mean crushing force of the off-the-shelf composite tube by minimum of 14% to the maximum of 38% and indicates a promising benefit towards enhancing the composite structures energy absorption.
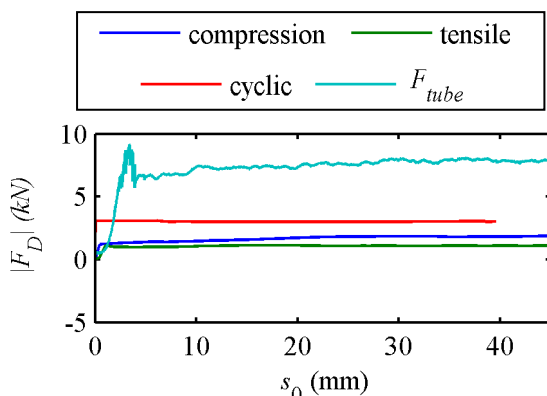
Fig. 13. Comparison of peak to peak damping force from tensile, compression and cyclic loading tests to mean crushing force of an off-the-shelf composite tube

6 Conclusion

In this paper, MR fluids compatibility to directional enhancement of composite structures

energy absorption has been investigated. The intensive parametric studies indicate that the piston head radius is the key parameter in achieving high damping force, as compared to other identified design parameters. However, the increment of the piston head radius would result in large increase of the weight of MR damper with the length size retained, due to the increase of the MR fluids volume flow. Thus a balance of the piston head length, radius and the damper length size is required for high damping force without mass increase. As the settling distance of the flow at the edge of the electrodes has a minimum limit, the ratio between the distance of the laminar flow and the gap of flow channel highly affected the consistency of the damping force. In this study, it also suggested that the distance of the laminar flow should be less than half of the gap of flow channel.

In the experimental investigation, the force distribution behaviour coincides with the numerical parametric studies and data obtained from the tested MR damper manufacturer's specifications. Inconsistency of the force distribution occurred at the lower end of velocity regime and this was slowly diminished as the velocity increases. The maximum peak to peak damping force achieved by the tested damper was roughly two-fifths of the mean crushing force of an off-the-shelf composite tube with similar radius size of MR damper and 2mm thickness. Finally, the MR fluids and the damper have a significant potential to increase the directional enhancement of the composite structure energy absorption as demonstrated in this paper.

As the MR damper can sustain the velocity up to 200mm/s, further experimental study that involves the higher end of the velocity range is required to further validate the findings in this paper. This will then be followed by developing a controller that can dynamically control the MR damper based on the crushing force and ultimately towards the design of MR fluids embedded composite structures.

References

[1] Joosten MW, Dutton S, Kelly D, Thomson R and Johnson AF. Developing crashworthy composite

helicopter structures: A building block approach. *14th Australian International Aerospace Congress*, Melbourne, Australia.

[2] Felt DW, Hagenbuchle M and Liu J. Rheology of a magnetorheological fluid. *Journal of Intelligent Material Systems and Structures*, Vol. 7, pp 589-593, 1996.

[3] Dyke SJ, Spencer BF, Sain MK, Carlson JD. Modeling and control of magnetorheological dampers for seismic response reduction. *Smart Material and Structures*, Vol. 5, pp 565-575, 1996.

[4] Yang G, Spencer BF, Carlson JD and Sain MK. Large-scale MR dampers: Modeling and dynamic performance considerations. *Engineering Structures*, Vol. 24, pp 309-323, 2002.

[5] Yang G, Spencer BF, Jung H and Carlson JD. Dynamic modeling of large-scale magnetorheological damper systems for civil engineering applications. *Journal of Engineering Mechanics*, Vol. 130, pp 1107-1114, 2004.

[6] Choi Y and Wereley NM. Biodynamic response mitigation to shock loads using magnetorheological helicopter crew seat suspensions. *Journal of Aircraft*, Vol. 42, No. 5, pp 1288-1295, 2005.

[7] Heimenz GJ, Hu W and Wereley NM. Investigation of MR dampers for enhanced crashworthiness and vibration isolation of helicopter crew seats. *American Helicopter Society 63rd Annual Forum*, Virginia Beach, VA, USA, pp 1187-1202, 2007.

[8] Lord Corporation. http://www.lord.com/Products-and-Solutions/Magneto-Rheological-(MR)/MR-Store.xml.

[9] McLeish TCB, Jordan T and Shaw MT. Viscoelastic response of electrorheological fluids. *Rheol Acta*, Vol. 35, No. 3, pp 427-448, 1991.

Copyright Statement